Possible Sensing Ability of Boron Nitride Nanosheet and its Al– and Si–Doped Derivatives for Methimazole Drug by Computational Study

Vessally, Esmail*[+]***; Farajzadeh, Parya; Najafi, Ezzatollah***
Department of Chemistry, Payame Noor University, Tehran, I.R. IRAN

ABSTRACT: *In this research, we studied the most stable configurations, electronic properties, and interactions between pristine and Al- and Si-doped boron nitride nanosheet BNNS and the methimazole drug MM by using Density Functional Theory (DFT) calculations. The results indicate that MM can be physically interacting into the pristine while chemically interacts with Al- and Si-doped BNNS. With the weak interaction and low change in E_g between BNNS and MM, this system seems is not suitable for potential sensing while Si-doped BNNS indicates a suitable interaction and high change in E_g during absorption of MM; showing a good candidate for a sensing device. The Al-doped BNNS shows a strong interaction with MM that leads to a high recovery time; indicating this system is suitable for decomposition of MM.*

KEYWORDS: *Al- and Si-doped boron nitride BNNS; Nanosheet; Methimazole drug; Adsorption; Sensing ability; DFT; Drug delivery system.*

INTRODUCTION

Methimazole is a thionamide antithyroid drug that inhibits the synthesis of thyroid hormones [1-3]. It was first introduced as an antithyroid agent in 1949 and is now commonly used in the management of hyperthyroidism, particularly in those for whom more aggressive options such as surgery or radioactive iodine therapy are inappropriate [4,5]. Methimazole, MM, prevents the thyroid gland from producing too much thyroid hormone. The MM drug is used to treat hyperthyroidism (overactive thyroid). It is also used before thyroid surgery or for radioactive iodine treatment. The MM drug may also be used for purposes not listed in this medication. On a weight basis, MM is 10 times more potent than the other major antithyroid thionamide used in North America, propylthiouracil [5], and is the active metabolite of the pro-drug carbimazole, which is an antithyroid medication used in the United Kingdom and parts of the former British Commonwealth [3] Traditionally, MM has been preferentially used over propylthiouracil due to the risk of fulminant hepatotoxicity carried by the latter,15 with propylthiouracil being preferred in pregnancy due to a perceived lower risk of teratogenic effects. Despite documented teratogenic effects in its published labels [4,5] the true teratogenicity of MM appears to be unclear [6-8] and its place in therapy may change in the future. The methods that identify MM residue are very important from the environmental point of view. One of these identification methods is to applying the nanostructures in sensing the MM drug. The parts of our compounds that are named functional groups are active sites in the compounds.

* *To whom correspondence should be addressed.*
+ E-mail: vessally@pnu.ac.ir ; vessally@yahoo.com
1021-9986/2021/4/1001-1011 11/$/6.01

In the MM drug, three active sites including (i) S=C–, (ii) –NH and (iii) –NCH_3 moiety. Moreover, In BNNS, a more active site for interaction is the boron atom as a Lewis acid.

Boron Nitride NanoSheets (BNNSs) are structurally like the carbon nanosheets, CNSs. Significant attention has been dedicated to using BNNSs since their electronic properties are independent of chirality, which leads them suitable for possible chemical sensing applications [9]. Furthermore, the outstanding thermal and chemical stability [10], cytotoxicity [11], and biocompatibility [12] aspects of the BNNSs, as compared to the CNSs, have encouraged chemists to investigate their potential uses as modern tools in the nanomedicine, biological and therapeutic fields as well as their interaction with biomolecules [13]. The experimental and theoretical reports have shown that the chemical doping with some atoms made the BNNSs more sensitive and reactive toward various molecules [14]. For example, *Wang et al.* [15] have reported that Ge doped into (8,0) single-walled boron nitride improved the electronic properties of the boron nitride nanostructure and increased their adsorption sensitivity toward CO and NO as confirmed by the Density of States (DOS) and electrical charge density.

The toxicity of the BNNSs is the main problem for their application as a drug delivery device in biological systems. The sensing process, however, can happen in both the biological or nonbiological environments using BNNSs. Accordingly, the aim of this study is to study the sensing properties of BNNSs (pristine BNNSs, Al- and Si-doped BNNSs) in nonbiological environments where the toxicity of the BNNSs is not important. In this study, we chose B, Al, N, and Si– heteroatoms in order to the investigation of nanosheets *via* the interaction energies and possible sensing aspects of the BNNSs toward methimazole has been investigated using DFT.

COMPUTATIONAL DETAILS

The reliability of various DFT methods and levels is already evaluated for the study of bond dissociation energies, heats of formation, and geometrical parameters. Among all DFT methods, B3LYP, M06, and M06-2X often give more reasonable geometries and vibrational frequencies that are closest to those obtained from the Hartree–Fock (HF) method [16]. Thus, to find suitable interactions between the BNNS and methimazole MM, the DFT calculations were performed using the M06-2X method and 6-311G(d) basis sets, as implemented in the GAMESS program [17]. Recent studies have illustrated that the M06 and M06-2X density functional result in more reliable interaction energies, thermochemistry, and non-covalent interactions [18]. The molecular structures of complexes studied in the present work were very large for which we have to use 6-311G(d) basis sets. Vibration frequencies were also analyzed to confirm that all the optimized structures are local minima on the potential energy surface. The DOS and Partial Density of States (PDOS) were calculated for all the complexes by the GaussSum program [19]. To avoid the boundary effects, atoms at the ends of the nanotube are saturated with hydrogen atoms. Calculated adsorption energy (*E*ad) of MM drug is defined as follows:

$$E_{ad} = E_{(methimazole/BNNS)} - (E_{methimazole} + E_{BNNS}) + E_{BSSE} \quad (1)$$

where *E(*methimazole*/*BNNS*)* is the total energy of the methimazole drug adsorbed on the pristine nanotube, *E(*methimazole*)* is the total energy of the methimazole molecule and *E*BNNS corresponds to the total energy of the isolated BNNS. *E*BSSE is the Basis Set Superposition Error (BSSE) energy and was obtained by the Boys–Bernardi counterpoise method [20]. To determine the sensitivity of the nanosheet, the change of the HOMO–LUMO energy gap (*E*g) was determined by

$$E_g = [(Eg2 - Eg1)/Eg1] \times 100 \quad (2)$$

where *E*g1 and *E*g2 are the values of the *E*g for BNNS and the methimazole/BNNS complex, respectively. Also, HOMO and LUMO are the highest-occupied molecular orbital and the lowest-unoccupied molecular orbital, respectively. The HOMO-LUMO gap is the difference between LUMO and HOMO that showed with E_g [21-40]. To ensure the lowest energy for the BNNS/MM complex rather than a local minimum, the Potential Energy Surface (PES) scans were performed with respect to various dihedral angles (*D*). For example, the dihedral angle was scanned and relative total energies were determined. All the calculations were done in the gas phase.

RESULTS AND DISCUSSION

Following the investigation of researchers in different fields of organic compounds [41-78] here, **s**ensing ability

of boron nitride nanosheet and its Al– and Si-doped derivatives for methimazole drug were investigated.

The pristine BNNS nanosheet

To study the adsorption process and sensing characters of the BNNSs, the interactions between pristine BNNS in different positions and MM (molecular formula $C_4H_6N_2S$) were investigated. In this study, the zigzag single-walled BNNS with a bond length of 1.45 Å was used to study the electronic properties (Fig. 1a). The value of HOMO and LUMO levels for BNNS are -0.306 and -0.012 a.u., respectively. The HOMO-LUMO gap is 7.98 eV which indicates an insulator material. Therefore, doping with metal or semimetal atoms would be useful to change BNNS to a semiconductor device.

The AlBNNS nanosheets

The interactions between Al-doped BNNS in different positions and MM were examined (Fig. 1b). The bond length of Al-N in Al-doped BNNS is 1.74 Å which goes out of the plane because of the large bond distance. The value of HOMO and LUMO levels for BNNS are -0.305 and -0.022, respectively. The calculations show that the LUMO level stabilized with Al-doping instead of the B atom while the HOMO level does not change significantly. The HOMO-LUMO gap is decreased to 7.70 eV with respect to BNNS which indicates a slight semiconductor character.

The SiBNNS nanosheets

The interactions between Si-doped BNNS and MM were investigated in different directions (Fig. 1c). The bond length of Si-N in Si-doped BNNS is 1.72 Å which leads the Si atom to stretch out of the plane due to its large bond distance. The value of HOMO and LUMO levels for BNNS are -0.236 and -0.012, respectively. The calculations show that both the HOMO and LUMO levels stabilized with Si-doping instead of the B atom. The HOMO-LUMO gap is considerably decreased to 6.09 eV with respect to BNNS which indicates a semiconductor character.

The Mulliken population analysis shows that 0.42 , 0.62 and 0.70 electrons transfer from the B, Si, and Al atoms to the N atom, clearly indicating the asymmetry of valence electron density and the ionic like bonding between B–N atoms in the BNNS, SiBNNS, and AlBNNS nanosheets. The Mulliken population analysis also

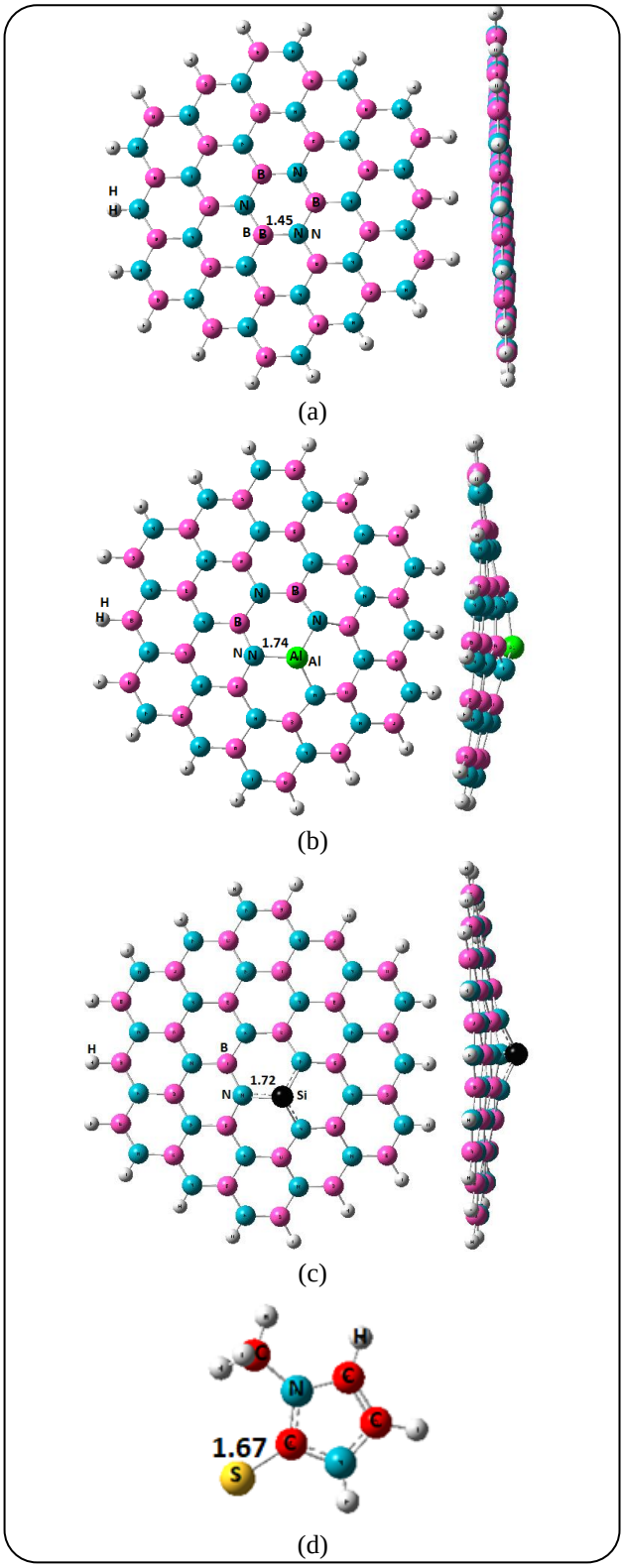

Fig. 1: Schematic view of the BNNS , AlBNNS , SiBNNS nanosheet. (a) The BBNS nanosheet; (b) The AlBNNS nanosheet; (c) The SiBNNS nanosheet; (d) The methimazole drug $C_4H_6N_2S$; The unit of the bond length is Å.

indicates that the B, Si, and Al atoms have a positive charge as a Lewis acid that Lewis base such as atoms with lone pair can attack to these sites.

The sensing ability of optimized pristine BNNS

The MM molecule has three active sites including the (i) S=C–, (ii) –NH and (iii) –NCH_3 moiety which NCH_3 has the steric effects that are not considered. The spontaneous interaction of S=C–active site with BNNS leads to both vertical and parallel interactions between the MM molecule and BNNS (Fig. 2). Further, other kinds of the interaction of MM include approach from its –NH group to the boron atoms of the pristine BNNS which is unstable with respect to the most stable complex about +10.23 kcal/mol. In BNNS/MM*, a vertical interaction occurs between the sulfur atom of S=C– in MM drug and boron atom of BNNS results in a less stable complex (Fig. 2a). In BNNS/MM, a parallel interaction happens between the sulfur atom of S=C– in MM drug and boron atom of BNNS results in a more stable complex (Fig. 2a). This complex of BNNS/MM is more stable than that of BNNS/MM* about -3.9 kcal/mol. Therefore, the most stable complex is BNNS/MM, wherein the MM drug aligns parallel to the BNNS surface which the corresponding adsorption energies is –14.24 kcal/mol (Table 1). This interaction leads that the bond lengths of the C=S group slightly increased from 1.67 in MM to 1.68 Å in the complex which indicates a weak interaction between MM and BNNS that bond distance of (S….B) is 3.29 Å. Another interaction is related to –NH in MM and the B atom of BNNS which the calculated data reveals that this interaction is not stable with respect to the most stable BNNS/MM.

The HOMO is more focused on the sulfur atom of C=S moiety in MM indicating that the MM molecule donates electron pairs from its sulfur atoms to the electron-deficient boron atom in BNNS surface in where the LUMO level is formed on the boron atoms of the BNNS surface (Fig. 3a).

There are two factors in the sensing process of MM by BNNS nanoparticles that the Ead and Eg parameters affect these sensing characters. The adsorption of MM onto BNNS may be reversible if the Ead is in a reasonable range (20-30 kcal/mol). Strong interactions are not favorable in drug sensing because of a long recovery time and thus hard desorption of a drug over a nanoparticle. With the more negative Ead, the recovery time (τ) is increased and this may be determined using the following equation [21]:

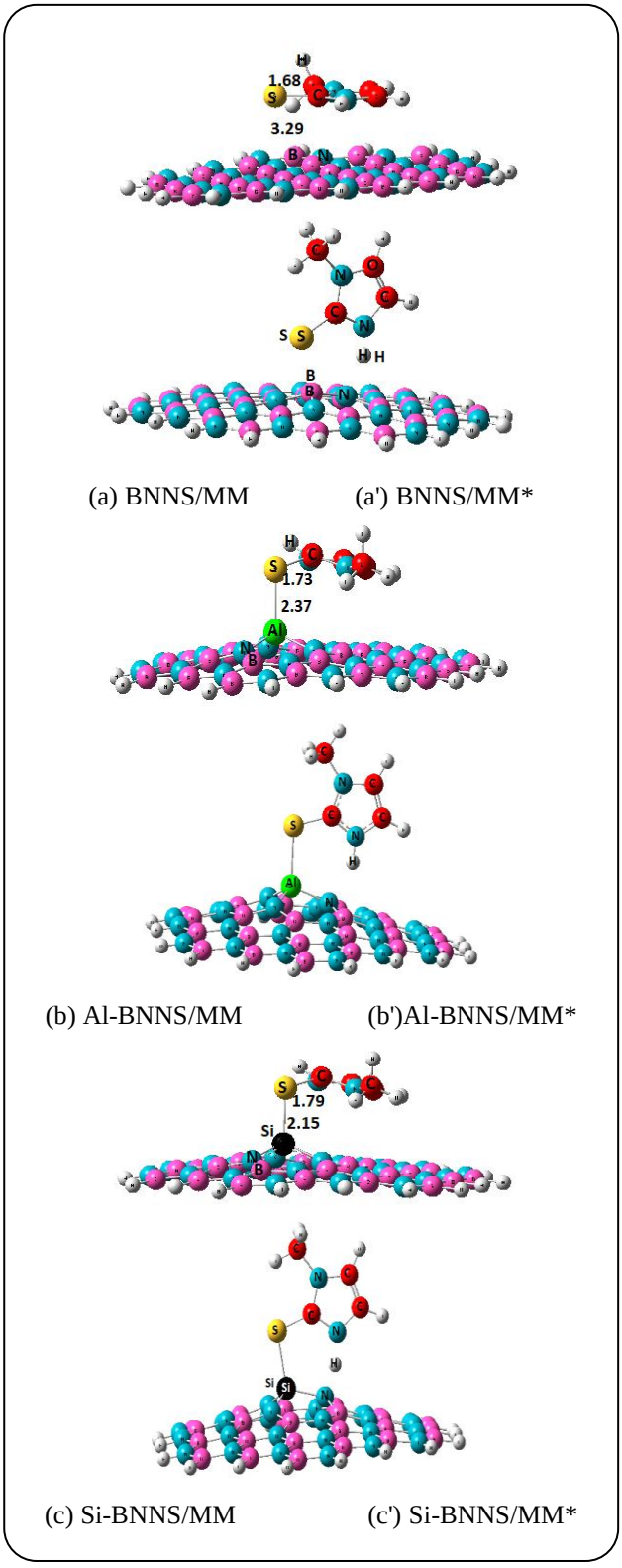

Fig. 2: The obtained stable configurations of complexes; (a) BNNS/MM or /MM* (b) AlBNNS/MM or MM* (c) SiBNNS/MM or MM* nanosheets. The unit of the bond length is Å.

$$\tau = \nu_0^{-1} \exp\left(-E_{ad}/kT\right) \quad (3)$$

Where v_0 is the attempt frequency, T is temperature and k is the Boltzmann's constant. According to this equation, the more negative the E_{ad}, the recovery time would increase in an exponential manner. The calculated E_{ad} of MM on the BNNS system is (-14.24 kcal/mol) the recovery time (τ) of the sensor is shorter. Under vacuum (or extreme) if UV light ($\upsilon \sim 3 \times 1014$ s−1) is applied for the recovery of MM from the surface of BNNS system, the recovery time is about 3.9 ×10−2 s. This further suggests that the recovery time is suitable at M06–2X level. However, because of the weak interaction of -14.24 kcal/mol in BNNS/MM, this system seems is not suitable for potential sensing of BNNS.

The second most important factor in sensing character is the HOMO–LUMO energy gap (E_g) of BNNS nanotubes in the presence of the MM. It has been shown that the E_g is proportional to the conduction electron population (σ) (presented in Eq. 4). The conduction electron population (σ) increases when HOMO–LUMO energy gap (E_g) decreases with the absorption of MM over BNNS. On the other hand, when the $-\%\Delta E_g$ increases, the sensing potential also increases. The correlation between E_g and the electrical conductance of nanostructures is as follows:

$$\sigma = AT^{3/2} \exp\left(-E_g/2kT\right) \quad (4)$$

Where k is the Boltzmann's constant, and A (electrons/$m^3K^{3/2}$) is a constant. There is an acceptable correlation between the obtained results of this procedure and experimental techniques [22].

Table 1 presents the E_g and $\%\Delta E_g$ values for adsorption of MM over BNNS which indicates that the $-\%\Delta E_g$ (11.96%) is for BNNS/MM complex; indicating that the BNNS is not a promising candidate for a potential sensor to detect MM.

The adsorption of MM on the Al-doped nanosheet

To study the suitable adsorption of the MM drug to BNNSs and to understand the effect of electronic structure and reactivity, the Al-doped BNNSs were examined. The Al atom has larger atomic radios as compared to the B atom, accordingly, the Al atoms tend to be pulled out from the nanosheet to reduce the torsion with re-hybridization from sp^2 to sp^3 which lets BNNS for the more reachable surface to interact with the MM molecule. The MM molecule with various positions of interactions was placed on the local area of the doped Al atom in Al-BNNS. Optimized structures of the Al–BNNS/MM and Al–BNNS/MM* complexes are displayed in Fig. 2b. According to interaction energies, in the most stable structure, the MM drug adsorbs strongly through the sulfur atom of S=C- group on the Al–BNNS with an adsorption energy of –43.84 kcal/mol. The bond distance of Al…S becomes 2.39 and C-S bond increased from 1.67 to 1.73 which shows a strong interaction between MM and BNNS (Fig. 2b). In the other conformation, the MM drug adsorbs vertically through the sulfur atom of the S=C- group on the Al–BNNS which is unstable +4.08 kcal/mol (Fig. 2b). Further, the NBO (Natural Bond Orbital) analysis indicated a charge transfer of 0.27 e between Al-BNNS to MM and it confirms the strong interaction between MM and Al-BNNS. Indeed, in this interaction system, the sulfur atom of MM has an unlocalized electron pair that acts as a Lewis base which donates an electron to the Al atom (Lewis acid). Based on the molecular orbitals maps, the LUMO level is more localized on the dopant Al atom. In the most stable complex of MM/Al–BNNS, the five-membered ring in MM occurs parallel on Al-BNNS surface (Fig. 3b).

Two factors in the sensing process including E_{ad} and Eg could be studied for Al-BNNS/MM complex. The E_{ad} for the Al-BNNS/MM complex is –43.84 kcal/mol that shows a strong interaction between Al-BNNS and MM which leads to a high recovery time. Therefore, from an energy and recovery time point of view, the Al-BNNS/MM complex is not suitable for a sensing ability while this strong interaction implies that Al-BNNS is a candidate for decomposition of the MM drug. On the other hand, Eg and ΔEg(%) of Al-BNNS do not significantly change so that ΔEg(%) becomes -4.98 which indicates low sensitivity of Al-BNNS to the MM drug which confirmed the high E_{ad} result.

The adsorption of methimazole drug on the Si-doped nanosheet

To find a suitable system for sensing ability, the Si atom is replaced instead of the B atom in BNNS, and this Si-doping causes a local deformation in which the Si atom is projected out of the plane due to reducing the torsional strain.

Optimized structures of the Si–BNNS/MM and Si–BNNS/MM* complexes are presented in Fig. 2c.

Table 1. Adsorption energy (E_{ad}, kcal/mol) for methimazole from the surface of the BNNS, Al, Si-doped nanosheet. Energy of Fermi level (E_F), HOMO, and LUMO, and HOMO-LUMO energy gap (E_g) in eV. The ΔE_g indicates the change of E_g after the adsorption process.

Structure	E_{ad}	E_{HOMO}	E_F	E_{LUMO}	E_g	ΔE_g(%)	Q (e)
BNNS	---	-0.3056	-0.1589	-0.0122	7.98	---	---
Al-BNNS	---	-0.3050	-0.1634	-0.0219	7.70	---	---
Si-BNNS	---	-0.2362	-0.1243	-0.0124	6.09	---	---
BNNS/MM	-14.24	-0.2412	-0.1120	-0.0171	7.03	-11.96	0.11
BNNS/MM*	-10.34	-0.2362	-0.1244	-0.0126	6.08	-23.79	---
Al-BNNS/MM	-43.84	-0.2896	-0.1551	-0.0206	7.32	-4.98	0.27
Al-BNNS/MM*	-39.76	-0.2851	-0.1510	-0.0169	7.30	-5.26	---
Si-BNNS/MM	-20.42	-0.1647	-0.0894	-0.0142	4.09	-32.75	0.25
Si-BNNS/MM*	-16.21	-0.1600	-0.0850	-0.0101	4.08	-33.02	---

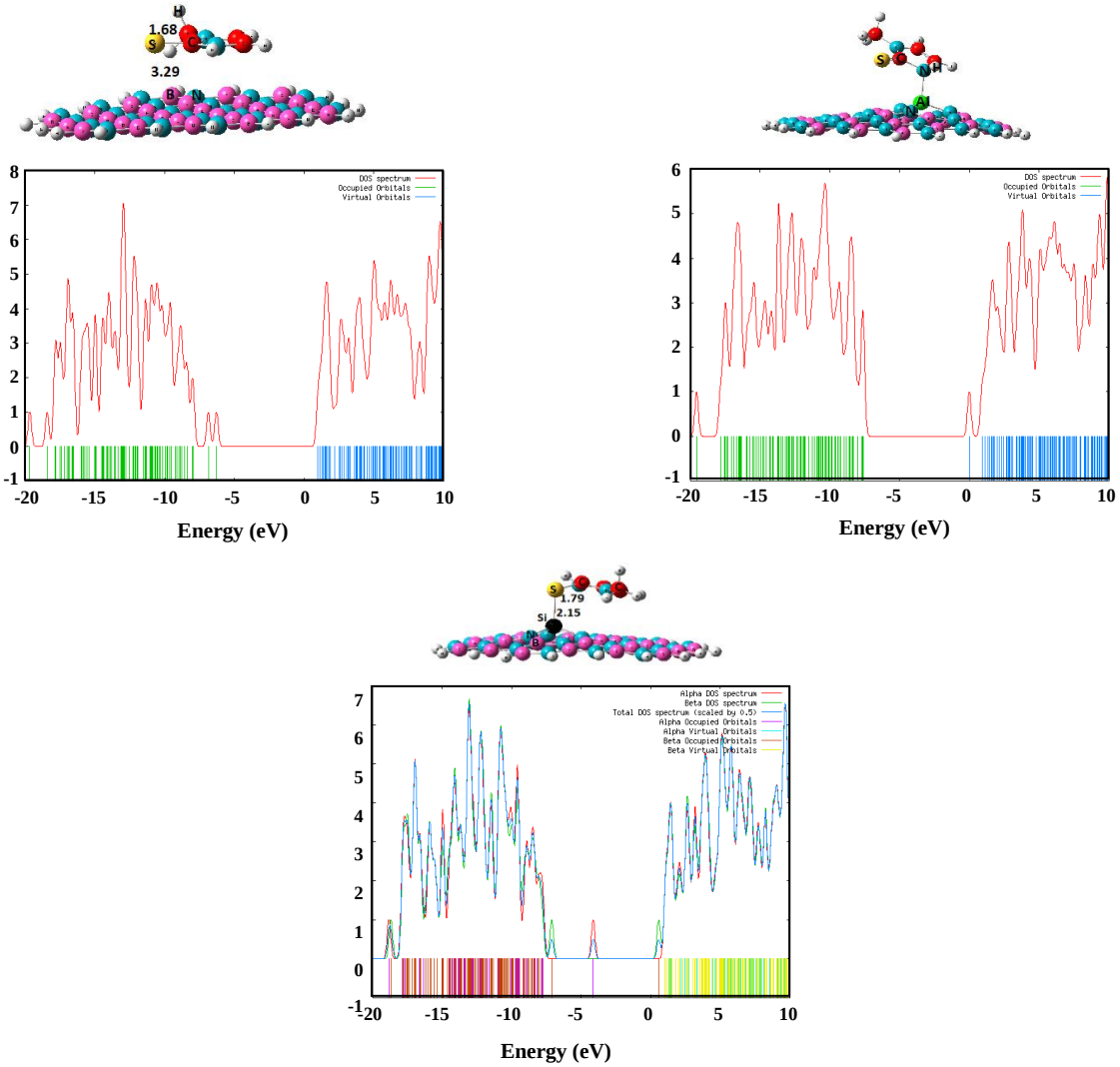

Fig. 3: The density of states (DOS) diagrams; (a) BNNS/MM (b) AlBNNS/MM (c) SiBNNS/MM nanosheets.

According to the adsorption energies, in the most stable structure, the MM drug adsorbs strongly through the sulfur atom of S=C- group on the Si–BNNS with adsorption energy of –20.42 kcal/mol. The bond distance of Si…S becomes 2.15 and C-S bond increased from 1.67 to 1.73 which shows a strong interaction between MM and BNNS (Fig. 2b). In the other conformation, the MM drug adsorbs vertically through the sulfur atom of the S=C- group on the Si–BNNS which is unstable +4.21 kcal/mol (Fig. 2c). Based on the molecular orbitals maps, the LUMO level is more localized on the Si atom. In the most stable complex of MM/Si–BNNS, the five-membered ring in MM occurs parallel on Si-BNNS surface.

Two factors in the sensing process including E_{ad} and E_g could be studied for Si-BNNS/MM complex. The E_{ad} for the Si-BNNS/MM complex is –20.42 kcal/mol that shows a suitable interaction between Si-BNNS and MM which leads to a short recovery time of 0.03 seconds according to Eq. 3. Therefore, the Si-BNNS/MM complex is a suitable case for being a sensing device. On the other hand, E_g and $\Delta E_g(\%)$ of Si-BNNS remarkably change so that $\Delta E_g(\%)$ be -32.75 that indicates the high sensitivity of Si-BNNS to the MM drug which also confirmed the suitable E_{ad} and recovery time.

The plot of the Partial Density of States (PDOS) individually shows the role of each part of the complex. In other words, PDOS shows the contributions of BNNS and MM in the complex. The Partial Density of States (PDOS) clearly indicates that a new level produced at the E_g gap of Si-BNNS mostly arises from MM interactions that leads to a decrease in E_g for BNNS/MM complex.

CONCLUSIONS

In the research, we have studied the stable configurations, electronic properties, and interactions between pristine and Al- and Si-doped boron nitride nanosheet BNNS and the methimazole drug MM by using DFT calculations. The results indicate that MM can be physically interacting into the pristine of -14.24 kcal/mol while chemically interacts with Al- and Si-doped BNNS. The weak interaction and low change in E_g between BNNS and MM, this system seems is not suitable for potential sensing while Si-doped BNNS indicates a suitable interaction of -20.42 kcal/mol and high change in E_g during absorption of MM; showing a good candidate for a sensing device. The Al-doped BNNS shows a strong interaction of -43.84 kcal/mol with MM that leads to a high recovery time; indicating this system is suitable for decomposition of MM. Finally, the scrutinized nanosheets are influenced by the number, size, filling patterns of the used heteroatoms.

Received : Jan. 2, 2021 ; Accepted : Feb. 22, 2021

REFERENCES

1] Burch H.B., Cooper D. S., Antithyroid Drug Therapy: 70 Years Later, *European Journal of Endocrinology*., **179(5)**: R261-R274 (2018).

[2] Manna D., Roy G., Mugesh G., Antithyroid Drugs and Their Analogues: Synthesis, Structure, and Mechanism of Action, *Acc, Chem Res.*, **46**: 2706-2715 (2013).

[3] David S., Cooper M.D., Antithyroid Drugs, *N. Engl. J. Med*. **352**: 905-917 (2005).

[4] Shafiei S., Davaran S., A Mini-Review on the Current COVID-19 Therapeutic Strategies, *Chem. Rev. Lett.* **3:**19-22 (2020).

[5] (c) Majedi S., Majedi S., Existing Drugs as Treatment Options for COVID-19: A Brief Survey of Some Recent Results, *J. Chem. Lett.*, **1:** 2-8(2020).

[6] Clark S.M., Saade G.R., Snodgrass W.R., Hankins G.D., Pharmacokinetics and Pharmacotherapy of Thionamides in Pregnancy, *Therapeutic Drug Monitoring.*, ***28*(4)**: 477-483 (2006).

[7] Cooper D.S., Laurberg P. Hyperthyroidism in pregnancy, *The Lancet Diabetes & Endocrinology*., **1(3):** 238-249 (2013).

[8] Mallela M.K., Strobl M., Poulsen R.R., Wendler C.C., Booth C.J., Rivkees S.A., Evaluation of Developmental Toxicity of Propylthiouracil and Methimazole, *Birth Defects Research Part B: Developmental and Reproductive Toxicology*, **101(4)**: 300-307 (2014).

[9] Eslami M., Vahabi V., Peyghan A.A., Sensing Properties of BN Nanotube Toward Carcinogenic 4-Chloroaniline: A Computational Study, *Physica E: Low-dimensional Systems and Nanostructures*., ***76***: 6-11 (2016).

[10] Ghassemi H.M., Lee C.H., Yap Y.K., Yassar R.S., In Situ TEM Monitoring of Thermal Decomposition in Individual Boron Nitride Nanotubes, *JOM.*, **62(4)**: 69-73 (2010).

[11] Ciofani G., Danti S., Ricotti L., D'Alessandro D., Moscato S., Berrettini S., Menciassi A., Boron Nitride Nanotubes: Production, Properties, Biological Interactions, and Potential Applications as Therapeutic Agents in Brain Diseases, *Current Nanoscience*., **7(1)**: 94-109 (2011).

[12] Zeng H., Zhi C., Zhang Z., Wei X., Wang X., Guo W., Golberg D., "White Graphenes": Boron Nitride Nanoribbons Via Boron Nitride Nanotube Unwrapping, *Nano Letters*., **10(12)**: 5049-5055 (2010).

[13] Peyghan A. A., Baei M. T., Moghimi M., Hashemian S., Adsorption and Electronic Structure Study of Imidazole on (6, 0) Zigzag Single-Walled Boron Nitride Nanotube, *Journal of Cluster Science*., **24(1)**: 31-47 (2013).

[14] Deng Z. Y., Zhang J. M., Xu K. W., Adsorption of SO_2 Molecule on Doped (8, 0) Boron Nitride Nanotube: A First-Principles Study, *Physica E: Low-dimensional Systems and Nanostructures*., **76**: 47-51 (2016).

[15] Wang R, Zhang D, Liu C. The Germanium-Doped Boron Nitride Nanotube Serving as a Potential Resource for the Detection of Carbon Monoxide and Nitric Oxide, *Comput Mater Sci.*,**82**: 361–366 (2014).

[16] (a) Hussain R., Imran M., Mehboob M. Y., Ali M., Hussain R., Khan M. U., Irfan A., Exploration of Adsorption Behavior, Electronic Nature and NLO Response of Hydrogen Adsorbed Alkali Metals (Li, Na and K) Encapsulated Al 1 2 N 1 2 Nanocages, *Journal of Theoretical and Computational Chemistry*., **19(08)**: 2050031 (2020)

(b) Mahmood A., Irfan A., Computational Analysis to Understand the Performance Difference Between Two Small-Molecule Acceptors Differing in Their Terminal Electron-Deficient Group, *Journal of Computational Electronics.*, **19(3)**: 931-939 (2020).

[17] Schmidt M.W., Baldridge K.K., Boatz J. A., Elbert S. T., Gordon M.S., Jensen J.H., Montgomery Jr J.A., General Atomic and Molecular Electronic Structure System, *Journal of Computational Chemistry*., **14(11):** 1347-1363 (1993).

[18] Zhao Y., Truhlar D. G., Density Functionals with Broad Applicability in Chemistry, *Accounts of Chemical Research*., **41(2)**: 157-167 (2008).

[19] O'boyle N. M., Tenderholt A. L., Langner K. M., Cclib: a Library for Package- Independent Computational Chemistry Algorithms, *Journal of Computational Chemistry*., **29(5)**: 839-845 (2008).

[20] Boys S. F., Bernardi F. J. M. P., The Calculation of Small Molecular Interactions by the Differences of Separate Total Energies, Some Procedures with Reduced Errors, *Molecular Physics*., **19(4)**: 553-566 (1970).

[21] Heravi M. R.P., Habibzadeh S., Ebadi A. G., Kheirollahi Nezhad P.D., Vessally E., Substituent Effects of Fused Hammick Silylenes Via Density Functional Theory Survey, *J. Phys. Org. Chem.*, **2021***:* e4264 (2021).

[22] Ma X., Kexin Z., Yonggang W., Ebadi A. G., Toughani M., Investigation of Low-Temperature Lipase Production and Enzymatic Properties of Aspergillus Niger, *Iran. J. Chem. Chem. Eng. (IJCCE),* Online from Jul. 7 (2021).

[23] Soleimani-Amiri S., Asadbeigi N., BadraghehbS., A Theoretical Approach to New Triplet and Quintet (nitrenoethynyl) alkylmethylenes,(nitrenoethynyl) alkylsilylenes,(nitrenoethynyl) alkylgermylenes, *Iran. J. Chem. Chem. Eng. (IJCCE).*, **39(4)**: 39-52 (2020).

[24] Zandieh S., Nami N., Hossaini Z., Ionic Liquid an Efficient Solvent and Catalyst for Synthesis of 1-aminoalkyl-2-naphthol and Naphthoxazine Derivatives, *Iran. J. Chem. Chem. Eng. (IJCCE).*, **38(4)**: 27-35 (2019).

[25] Ahmadi S., Hosseinian A., Delir Kheirollahi Nezhad P., Monfared A., Vessally E., Nano-Ceria (CeO2): An Efficient Catalyst for the Multi-Component Synthesis of a Variety of Key Medicinal Heterocyclic Compounds, *Iran. J. Chem. Chem. Eng. (IJCCE).*, **38(6)**: 1-19 (2019).

[26] Vessally E., Mohammadi S., Abdoli M., Hosseinian A., Ojaghloo P., Convenient and Robust Metal-Free Synthesis of Benzazole-2-Ones Through the Reaction of Aniline Derivatives and Sodium Cyanate in Aqueous Medium, *Iran. J. Chem. Chem. Eng. (IJCCE).*, **39(5)**: 11-19 (2020).

[27] Jalali Sarvestani M.R., Fullerene P., (C20) as a Potential Adsorbent and Sensor for the Removal and Detection of Picric Acid Contaminant: DFT Studies Charehjou, *Cent. Asian J. Environ. Sci. Technol. Innov*., **2**: 12-19 (2021).

[28] Heravi M. R. P., Hosseinian A., Rahmani Z., Ebadi A., Vessally E., Transition- Metal- Catalyzed Dehydrogenative Coupling of Alcohols and Amines: a Novel and Atom- Economical Access to Amides, *J. Chin. Chem. Soc*., **68(5)**: 723-737(2021).

[29] Xu W., Guo D., Ebadi A. G., Toughani M., Vessally E., Transition-Metal Catalyzed Carboxylation of Organoboron Compounds with CO_2, *Journal of CO_2 Utilization.*, **45**: 101403 (2021).

[30] Hassanpour A., Heravi M. R. P., Ebadi A., Hosseinian A., Vessally E., Oxidative Trifluoromethyl (thiol/selenol) ation of Terminal Alkynes: An Overview, *Journal of Fluorine Chemistry*., 109762 (2021).

[31] Kareem R.T., Azizi B., Asnaashariisfahani M., Ebadi A., Vessally E., Vicinal Halo-Trifluoromethylation of Alkenes, *RSC Advances*., **11(25)**: 14941-14955 (2021).

[32] Azizi B., Heravi M.R.P., Hossaini Z., Ebadi A., Vessally E., Intermolecular Difunctionalization of Alkenes: Synthesis of B-Hydroxy Sulfides, *RSC Adv*., **11**: 13138-13151(2021).

[33] Xu W., Ebadi A. G., Toughani M., Vessally E., Incorporation of CO_2 into Organosilicon Compounds Via Csi Bond Cleavage, *Journal of CO_2 Utilization*., 101358 (2020).

[34] Liu Z., Ebadi A., Toughani M., Mert N., Vessally E., Direct Sulfonamidation of (Hetero)Aromatic C–H Bonds with Sulfonyl Azides: A Novel and Efficient Route to N-(Hetero)Aryl Sulfonamides, *RSC Adv.*, **10**: 37299-37313 (2021).

[35] Liu Y., Ebadi A. G., Youseftabar-Miri L., Hassanpour A., Vessally E., Methods for Direct C (sp 2)–H Bonds Azidation, *RSC Advances*., **9(43)**: 25199-25215 (2019).

[36] Rasouli A., Bafkar A., Chaghakaboodi Z., Kinetic and Equilibrium Studies of Adsorptive Removal of Sodium-Ion onto Wheat Straw and Rice Husk Wastes, *Sci. Technol. Innov*., **1**: 310-329 (2020).

[37] Ali A., Iqbal M., Waheed A., Co-Treatment of Chlorophenol and Methanolic Wastes, *Central Asian Journal of Environmental Science and Technology Innovation*., **1(5)**: 277-280 (2020).

[38] (a) Jalali Sarvestani M., Mert N., Vessally E., Cross-Dehydrogenative Coupling of Aldehydes with N-Hydroxyimides: an Efficient and Straightforward Route to N-Hydroxyimides Esters, *J. Chem. Lett..*, **1(3)**: 93-102 (2020).
DOI: 10.22034/jchemlett.2020.120304

(b) Vessally E., Behmagham F., Metal-Free Regioselective Thiocyanation of (Hetero) Aromatic C-H Bonds Using Ammonium Thiocyanate: an Overview, *J. Chem. Lett.*, **1**: 25-31(2020).
DOI: 10.22034/jchemlett.2020.107760

(c) Abdulkareem Mahmood E., Azizi B., Majedi S., Decarboxylative Cyanation and Azidation of Carboxylic Acids: an Overview, *Chem. Rev. Lett.*., **3(1)**: 2-8 (2020).
DOI: 10.22034/jchemlett.2020.120304

(d) Salehi N., Azizi B., Electrochemical Double Carboxylation of Unsaturated C-C Bonds with Carbon Dioxide: an Overview, *J. Chem. Lett.*., **2(1)**: 2-8 (2021).
DOI: 10.22034/jchemlett.2021.275293.1023

(e) Tayde D., Lande M., Synthesis of 2, 4 Disubstituted 1, 5 Benzodiazepines Promoted by Efficient Silica-Alumina Catalyst, *Chem. Rev. Lett.*., **4(1)**: 30-36 (2021).
DOI: 10.22034/crl.2020.255303.1089

(f) Bakhtiary A., Heravi M.R.P., Hassanpour A., Amini I., Vessally E., Recent Trends in the Direct Oxyphosphorylation Of C–C Multiple Bonds, *RSC Adv*., **11**, 470-483 (2021).

[39] Sreerama L., Vessally E., Behmagham F., Oxidative Lactamization of Amino Alcohols: An Overview, *J. Chem. Lett*., **1**: 9-18 (2020).

[40] (a) Majedi S., Behmagham F., Vakili M., Theoretical View on Interaction Between Boron Nitride Nanostructures and Some Drugs, *J. Chem. Lett.*., **1(1)**: 19-24 (2020).

(b) Jalali Sarvestani M., Majedi S., A DFT Study on the Interaction of Alprazolam with Fullerene (C20), *J. Chem. Lett.*., **1(1)**: 32-38 (2020).

(c) Kamel M., Morsali A., Raissi H., Mohammadifard K., Theoretical Insights into the Intermolecular and Mechanisms of Covalent Interaction of Flutamide Drug With COOH and COCL Functionalized Carbon Nanotubes: A DFT Approach, *Chem. Rev. Lett.*., **3(1)**: 23-37 (2020).

(d) Jalali Sarvestani M., Ahmadi R., Farhang Rik B., Procarbazine Adsorption on The Surface of Single Walled Carbon Nanotube: DFT Studies, *Chem. Rev. Lett.*., **3(4)**: 175-179 (2020).

(e) Jalali Sarvestani M., Doroudi Z., Fullerene (C20) as a Potential Sensor for Thermal and Electrochemical Detection of Amitriptyline: A DFT Study, *J. Chem. Lett.*, **1(2)**: 63-68 (2020).

(f) Doroudi Z., Jalali Sarvestani M., Boron Nitride Nanocone as an Adsorbent and Senor for Ampicillin: A Computational Study, *Chem. Rev. Lett.*., **3(3)**: 110-116 (2020).

[41] Ejeh S., Uzairu A., Shallangwa G., Abechi S., Computational Techniques in Designing a Series of 1,3,4-Trisubstituted Pyrazoles as Unique Hepatitis C Virus Entry Inhibitors, *Chem. Rev. Lett.*., **4(2)**: 108-119 (2021).

[42] Shajari N., Yahyaei H., Ramazani A., Experimental and Computational Investigations of Some New Cabamothioate Compounds, *Chem. Rev. Lett.*., **4(1)**: 21-29 (2021).

[43] Kamel M., Mohammadifard K., Thermodynamic and Reactivity Descriptors Studies on the Interaction of Flutamide Anticancer Drug with Nucleobases: a Computational View, *Chem. Rev. Lett.*, **4(1)**: 54-65 (2021).

[44] Hashemzadeh B., Edjlali L., Delir Kheirollahi Nezhad P., Vessally E., A DFT Studies on a Potential Anode Compound for Li-Ion Batteries: Hexa-Cata-Hexabenzocoronene Nanographen. *Chem. Rev. Lett.* (2020).

[45] Salehi N., Vessally E., Edjlali L., Alkorta I., Eshaghi M., Nan@Tetracyanoethylene (n=1-4) Systems: Sodium Salt vs Sodium Electride, *Chem. Rev. Lett.*., **3(4)**: 207-217 (2020).

[46] Liu Y., Xu T., Liu Y., Gao Y., Di C., Wear and Heat Shock Resistance of Ni-WC Coating on Mould Copper Plate Fabricated by Laser, *Journal of Materials Research and Technology.*, **9(4)**: 8283-8288 (2020).

[47] Zhang H., Guan W., Zhang L., Guan X., Wang S., Degradation of an Organic Dye by Bisulfite Catalytically Activated with Iron Manganese Oxides: The Role of Superoxide Radicals, *ACS omega*., **5(29):** 18007-18012 (2020).

[48] Zhang H., Sun M., Song L., Guo J., Zhang L., Fate of NaClO and Membrane Foulants During in-Situ Cleaning of Membrane Bioreactors: Combined Effect on Thermodynamic Properties of Sludge, *Biochemical Engineering Journal*., **147**: 146-152 (2019).

[49] Sun M., Yan L., Zhang L., Song L., Guo J., ... Zhang H., New Insights into the Rapid Formation of Initial Membrane Fouling after In-Situ Cleaning in a Membrane Bioreactor, *Process Biochemistry* (1991)., **78**: 108-113 (2019).

[50] Wang Q., Sun S., Zhang X., Liu H., Sun B., Guo S., Influence of Air Oxidative and Non-Oxidative Torrefaction on the Chemical Properties of Corn Stalk, *Bioresource Technology.*, ***332***: 125120 (2021).

[51] Liu J., Ren M., Lai X., Qiu G., Iron-Catalyzed Stereoselective Haloamidation of Amide-tethered Alkynes, *Chemical Communications (Cambridge, England)*., **57(35)**: 4259-4262 (2021).

[52] Duan Y., Liu Y., Chen Z., Liu D., Yu E., Zhang X., Du H., Amorphous Molybdenum Sulfide Nanocatalysts Simultaneously Realizing Efficient Upgrading of Residue and Synergistic Synthesis of 2D MoS_2 Nanosheets/Carbon Hierarchical Structures, *Green Chemistry: An International Journal and Green Chemistry Resource: GC.*, **22(1)**: 44-53 (2020).

[53] Pang X., Gong K., Zhang X., Wu S., Cui Y., Qian B., Osteopontin as a Multifaceted Driver of Bone Metastasis and Drug Resistance, *Pharmacological Research*., **144**: 235-244 (2019).

[54] Xu J., Ji L., Ruan Y., Wan Z., Lin Z., Xia S., Cai X., UBQLN1 Mediates Sorafenib Resistance Through Regulating Mitochondrial Biogenesis and ROS Homeostasis by Targeting PGC1β in Hepatocellular Carcinoma, *Signal Transduction and Targeted Therapy.*, **6(1)**: 190 (2021).

[55] Yang Y., Chen H., Zou X., Shi X., Liu W., Feng L., Chen Z., Flexible Carbon-Fiber/Semimetal Bi Nanosheet Arrays as Separable and Recyclable Plasmonic Photocatalysts and Photoelectrocatalysts, *ACS Applied Materials & Interfaces*., **12(22)**: 24845-24854 (2020).

[56] Pan X., Wei J., Zou M., Chen J., Qu R., Wang Z., Products Distribution snd Contribution of (de)Chlorination, Hydroxylation and Coupling Reactions to 2,4-Dichlorophenol Removal in Seven Oxidation Systems, *Water Research (Oxford)*., **194**: 116916 (2021).

[57] Zou M., Qi Y., Qu R., Al-Basher G., Pan X., Wang Z., Zhu F., Effective Degradation of 2,4-Dihydroxybenzophenone by Zero–Valent Iron Powder (Fe0)-Activated Persulfate in Aqueous Solution: Kinetic Study, Product Identification and Theoretical Calculations, *The Science of the Total Environment*., **771**: 144743 (2021).

[58] Cao W., Wu N., Qu R., Sun C., Huo Z., Ajarem J. S., Zhu F., Oxidation of Benzophenone-3 In Aqueous Solution by Potassium Permanganate: Kinetics, Degradation Products, Reaction Pathways, and Toxicity Assessment, *Environmental Science and Pollution Research.*, 1-11(2021).

[59] Lv X., Liu Y., Xu, S., Li Q., Welcoming Host, Cozy House? the Impact of Service Attitude on Sensory Experience, *International Journal of Hospitality Management.*, **95**: 102949 (2021).

[60] Liu Y., Lv X., Tang Z., The Impact of Mortality Salience on Quantified Self Behavior During the COVID-19 Pandemic, *Personality and Individual Differences*., **180**: 110972 (2021).

[61] Yang Y., Liu Y., Lv X., Ai J., Li Y., Anthropomorphism and Customers' Willingness to Use Artificial Intelligence Service Agents, *Journal of Hospitality Marketing & Management*., 1-23 (2021).

[62] Zhang L., Zhang M., You S., Ma D., Zhao J., Chen Z., Effect of Fe^{3+} on The Sludge Properties and Microbial Community Structure in a Lab-Scale A_2O Process, *The Science of the Total Environment*., **780**: 146505 (2021).

[63] Zhang. L., Zheng J., Tian S., Zhang H., Guan X., Zhu S., Li Z., Effects of Al^{3+} on The Microstructure and Bioflocculation of Anoxic Sludge, *Journal of Environmental Sciences (China).*, **91**: 212-221 (2020).

[64] Zhao H., Liu X., Yu L., Lin S., Zhang C., Xu H., Wang L., Comprehensive Landscape of Epigenetic-Dysregulated Lncrnas Reveals a Profound Role of Enhancers in Carcinogenesis in BC Subtypes, *Molecular Therapy-Nucleic Acids*, **23**: 667-681 (2021).

[65] Cheng J., Tan Z., Xing Y., Shen Z., Zhang Y., Liu L., Liu S., Exfoliated Conjugated Porous Polymer Nanosheets for Highly Efficient Photocatalytic Hydrogen Evolution, *Journal of Materials Chemistry, A, Materials for Energy And Sustainability*, **9(9)**: 5787-5795 (2021).

[66] Dong P., Zhang T., Xiang H., Xu X., Lv Y., Wang Y., Lu C., Controllable Synthesis of Exceptionally Small-Sized Superparamagnetic Magnetite Nanoparticles for Ultrasensitive MR Imaging and Angiography, *Journal of Materials Chemistry. B, Materials for Biology and Medicine.*, **9(4)**: 958-968 (2021).

[67] Wang Z., Zhang T., Pi L., Xiang H., Dong P., Lu C., Jin T., Large-Scale One-Pot Synthesis of Water-Soluble and Biocompatible Upconversion Nanoparticles for Dual-Modal Imaging, *Colloids and Surfaces, B, Biointerfaces.*, **198**: 111480 (2021).

[68] Zhuo Z., Wan Y., Guan D., Ni S., Wang L., Zhang Z., Zhang B.T., A Loop- Based and AGO- Incorporated Virtual Screening Model Targeting AGO- Mediated miRNA–mRNA Interactions for Drug Discovery to Rescue Bone Phenotype in Genetically Modified Mice, *Advanced Science.*, ***7*(13)**: 1903451 (2020).

[69] Deng X., Xu T., Huang G., Li Q., Luo L., Zhao Y., ... Zhu B., Design and Fabrication of a Novel Dual-Frequency Confocal Ultrasound Transducer for Microvessels Super-Harmonic Imaging, *IEEE Transactions on Ultrasonics, Ferroelectrics, and Frequency Control*., **68(4)**: 1272-1277 (2020).

[70] Wang R., Yuan Y., Zhang J., Zhong X., Liu J., Xie Y., ... Xu Z., Embedding Fe_2P Nanocrystals in Bayberry-Like N, P-Enriched Carbon Nanospheres as Excellent Oxygen Reduction Electrocatalyst for Zinc-Air Battery, *Journal of Power Sources*., **501**: 230006 (2021).

[71] Li H., Xu B., Lu G., Du C., Huang N., Multi-Objective Optimization of PEM Fuel Cell by Coupled Significant Variables Recognition, Surrogate Models and a Multi-Objective Genetic Algorithm, *Energy Conversion and Management*, **236**: 114063 (2021).

[72] Li H., Gao Y., Du C., Hong W., Numerical Study on Swirl Cooling Flow, Heat Transfer and Stress Characteristics Based on Fluid-Structure Coupling Method Under Different Swirl Chamber Heights and Reynolds Numbers, *International journal of heat and mass transfer.*, **173**: 121228 (2021).

[73] Wang S., Zhao Y., Li J., Lai H., Qiu C., Pan N., ... Gong Q., Neurostructural Correlates of Hope: Dispositional Hope Mediates the Impact of the SMA Gray Matter Volume on Subjective Well-Being in Late Adolescence, *Social cognitive and Affective Neuroscience*., **15(4)**: 395-404 (2020).